Journal of Sound and Vibration 395 (2017) 258–271

Contents lists available at ScienceDirect

Journal of Sound and Vibration

journal homepage: www.elsevier.com/locate/jsvi

Characterizing the robustness and susceptibility of steady-state dynamics in post-buckled structures to stochastic perturbations

Ryan L. Harne *, Quanqi Dai

Department of Mechanical and Aerospace Engineering, The Ohio State University, Columbus, OH 43210, USA

ARTICLE INFO

Article history:
Received 19 March 2016
Received in revised form
16 November 2016
Accepted 4 February 2017
Handling Editor: A.V. Metrikine
Available online 11 February 2017

Keywords:
Post-buckled structure
Vibration
Snap-through
Robustness
Stochastic oscillations
Stochastic resonance

ABSTRACT

Recent reports exemplify both the potential and the concerns encountered in implementing post-buckled structures in diverse applications. By numerical and experimental methods, characterizations have provided useful insights on the dynamic sensitivities of such bi- or multistable structures subjected to either harmonic or stochastic excitations. Yet, the more realistic scenario of combined harmonic and stochastic loading has been not been closely examined so that such sensitivities might be fully illuminated. To provide a more complete understanding on the robustness and susceptibility of multistable structures to dynamic state transitions, this research establishes new analytical and experimental methods to quantify the likelihood of triggering transitions among dynamic regimes of an archetypal post-buckled structure as a result of combined harmonic and stochastic loading. It is discovered that persistent periodic snap-through dynamics are rapidly disabled by additional noise excitation when the harmonic excitation contribution occurs at frequencies close to the linearized resonance. The extra noise may also drastically compromise the integrity of small-amplitude periodic responses that occur at frequencies around one-half of the linearized resonance. Particular relative proportions of the noise standard deviation and harmonic excitation amplitude are uncovered that most readily compromise the robustness of a given steady-state dynamic regime. The analytical method also complements prior developments focused on stochastic resonance by uncovering the broader perspective of dynamic sensitivities of post-buckled structures under arbitrary combinations of harmonic and random driving loads.

1. Introduction

Snap-through is the dynamic response associated with displacements from one stable equilibrium to another in a bistable, multistable, or post-buckled structure, and it results in a large sudden conversion between potential and kinetic energy that is dissipated in time by damping effects [1]. This unique, nonlinear dynamic behavior is important for a variety of engineering applications. Persistent snap-through oscillations are favorable for harvesting ambient vibration energies as a sustainable electrical power resource using bistable electromechanical devices. Namely, when the exciting energies are insufficient to greatly drive a linear energy harvesting platform, the same inputs may induce stochastic resonance-like

* Corresponding author.
E-mail address: harne.3@osu.edu (R.L. Harne).

http://dx.doi.org/10.1016/j.jsv.2017.02.006
0022-460X/

behaviors in bistable systems, promoting energetic oscillations and considerable electric power production [2–4]. Transitions among post-buckled states also facilitates novel, adaptive capabilities for engineered structures, including tunable frequency sensitivities [5], graded energy absorption features [6–8], exceptional actuation authority [9], and large multistable shape morphing [10]. Yet, considered from the lens of different applications, snap-through can be detrimental to the integrity and performance of critical structural systems. For example, aircraft may be subjected to skin buckling due to combined thermal and mechanical loading on the thin surface panels and control surfaces [11]. Such bi- or multistability could rapidly compromise system integrity if repeated dynamic transitions among the stable equilibria are activated [12,13]. Thus, archetypal, slender aircraft components have earned a recent focus towards developing predictive tools that inform deployment of such structural elements [14,15]. Indeed, wherever slender structural constituents are employed in engineering systems undergoing compressive loads there is the possibility that buckling may be induced at one or more locations, which poses a genuine concern for triggering snap-through events as a result of additional lateral stresses or loads [16].

Among these diverse investigations, the dynamics of *bistable structures* have been the focus of numerous investigations. The existence of two stable equilibria is amenable for *analytical methods* that yield general insights, albeit at a resolution viable for general engineering design guidance rather than exacting precision. Because more complex multistable structures do not involve a considerable change in the global dynamic behaviors that may result [17], bistable structures are a suitable substitute to investigate the fundamental dynamic phenomena and sensitivities of a whole class of engineering systems: structures with more than one statically stable equilibria.

As a result, a broad range of analytical studies have been undertaken on the structural dynamics of post-buckled structures and bistable oscillators to obtain important insights. Moon and Holmes [18] investigated an archetypal bistable cantilever that was buckled using magnetic forces, and employed analytical tools including Poincaré sections and Melnikov theory to yield important knowledge on the persistence of harmonically-excited steady-state motions. Later, Szemplińska-Stupnicka and Rudowski [19] utilized approximate analytical solutions to the governing equations via assumed sinusoidal response behavior to predict the onset of dynamic transitions in harmonically-excited bistable structures and the corresponding spectral energy distributions. Virgin [20] characterized the frequency sensitivities of archetypal mechanical and structural systems due to load and geometric constraints that could promote post-buckling, revealing that buckling is easily identified by the vanishing of the fundamental natural frequency. Recently, the idea of using bistable structures for vibration energy harvesting applications gave new motivation for analytical study that could uncover important knowledge for the harvester's best implementation. Thus, researchers have developed analyses that help identify methods for harnessing bistable energy harvesters in applications with harmonic [21,22] or stochastic exciting vibrations [23] that may be favorably converted into electric power. In an adaptive structure application, Kidambi et al. [7] used an analytical approach based on the harmonic balance method to elucidate the roles of symmetry, frequency, and excitation amplitude on the damping adaptation achieved by embedding a bistable constituent in an elastic mechanical system. Continued investigations are identifying the sensitivities of bistable structures under transient [24] or impulsive [25] conditions, which furthers the knowledgebase for effective utilization or operation of bistable engineering systems in a diverse range of applications. While this brief review is by no means comprehensive, the breadth of knowledge derived from *analytical studies on bistable structural dynamics* – particularly those incorporating supporting numerical or experimental evidence – has shed remarkable light and understanding on the dynamic behaviors unique to bistable systems but also manifest in the more complex multistable structural systems.

On the other hand, there is an important omission from this portfolio of knowledge. Although many scenarios involve harmonic or stochastic energies which drive or excite a post-buckled structure, it is rare that purely tonal or purely stochastic force/stress exists in the natural or engineered world. For instance, it is common that a background level of noise is not significantly less than spectral amplitude peaks associated with a mechanical or structural vibration response from harmonic inputs [26,27]. Considering the alternative perspective, even near-random excitations such as turbulent boundary layers past structural surfaces can induce vortex shedding that results in a periodic contribution to the total structural load [28]. More generally, some engineering systems, in particular aircraft [29,30], undergo an exhaustive variety of loading over the course of typical operations such that the structural components are at some times subjected to strongly tonal, mostly stochastic, or an even mixture of harmonic and stochastic excitations. While previous studies have analytically or numerically investigated the sensitivities of monostable nonlinear oscillators to such combined harmonic and stochastic excitations [31–35], there is a lack of comparative, analytically-based understanding for structures that possess more than one stable equilibrium. Thus, due to the myriad examples of post-buckled structures in modern and emerging engineering applications and the broad relevance of combined harmonic and stochastic inputs, the motivation of this research is to bridge the knowledge gap and lay a foundation for the study of harmonically- and stochastically-excited bistable structures using *new analytical* and *experimental methods* that yield conclusive insights.

The following section describes the model of the archetypal post-buckled structure examined in this work and the analytical framework employed to pursue understanding of the system behaviors in consequence to a combination of harmonic and stochastic excitation. The experimental system is then introduced and experimental results are compared to analytical predictions to correlate the conclusions from experiments to those suggested by the analysis. Concluding remarks summarize the principal findings of this research.

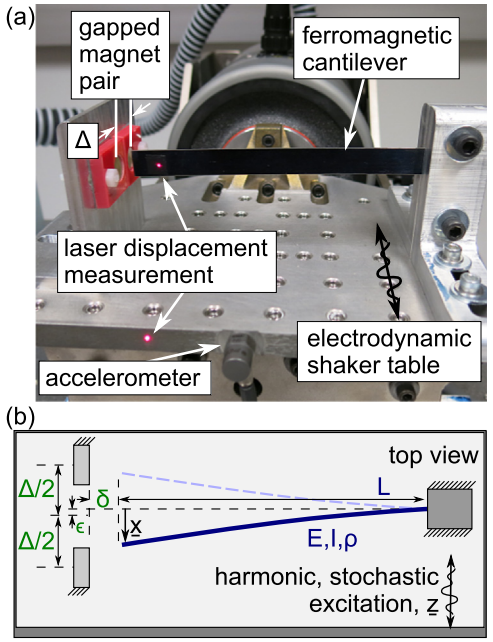

Fig. 1. (a) Photograph of experimental post-buckled cantilever and excitation method. (b) Schematic of experiment showing parameters for tuning of the bistability via magnet positioning.

2. Analytical investigation framework

2.1. Magnetoelastic bistable structure

Moon and Holmes [18] previously evaluated a harmonically-excited magnetoelastic beam due to its capability to exhibit the full range of dynamical behaviors associated with bistability, including strange attractors, 'coexisting' periodic motions, initial condition dependence, and multiple stable equilibria. This experimental platform also conveniently enables one to tune a broad range of relevant nonlinear and linear structural parameters by adjusting magnet positions. Over the years, this magnetoelastic bistable structure has received significant research attention due to such practical and theoretical versatility [36–38]. This research employs the same archetypal bistable structure, now instead with the broader focus of elucidating the cantilever response induced by excitations that are a combination of harmonic and stochastic energies. Fig. 1 provides a photograph and schematic of the experimental system. The platform includes a ferromagnetic spring steel cantilever with a gapped magnet pair positioned near the beam free tip. Due to the magnet pair positioning parameters δ and Δ, the cantilever is buckled such that the beam tip statically maintains one of two stable equilibria whereby the free tip points more towards one magnet than the other, illustrated in Fig. 1(b), which are the symmetric post-buckled stable states. Asymmetric post-buckled stable states may be realized using a non-zero offset parameter $\varepsilon \neq 0$, although such asymmetry was avoided in this research for sake of complying with the current analytical model formulation that presumes the combination of elastic and magnetic restoring forces on the cantilever are symmetric. The spring steel beam ($E=210$ GPa, $I=1.387\times10^{-13}$ m^4, $\rho=7800$ kg/m^3) has length $L=124$ mm from the clamped end while an electrodynamic shaker drives the beam clamped end and fixed magnets with a controlled base excitation signal.

2.2. Governing equation for cantilever displacement

For this archetypal post-buckled structure, the governing equations of motion are formulated using the basis that a single-mode Galerkin procedure is applied to the partial differential equation of motion to reduce it to a single ordinary differential equation of motion for the beam tip motion $\underline{x}$ proportional to the principal vibration response and relative to the moving base displacement $\underline{z}$ [16]. As a result, one has an equation

$$m\ddot{\underline{x}} + b\dot{\underline{x}} + k_1(1-p)\underline{x} + k_3\underline{x}^3 = -m\ddot{\underline{z}} \tag{1}$$

where m, b, k_1, k_3 are the single-mode contributions from the cantilever mass, viscous damping, linear, and nonlinear stiffness, and the load parameter p is related to the nonlinear influences of the magnets that induce buckling (i.e. when $p>1$) [18]. For axially-loaded structural systems, a similar parameter influence p appears in the governing equation related to the nearness of an applied axial force to the critical Euler buckling load in which case. For instance, considering a simply

supported beam, p is the ratio of the axial force to $\pi^2 EI/L^2$ [16]. In this magnetoelastic system, the magnetic influences also contribute to the linear and nonlinear stiffness terms k_1 and k_3. Here, the nonlinear stiffness contributions are truncated to retain only the cubic term from an infinite power series expansion to eliminate the intricate multistable responses, potentially enabled for higher-order stiffness terms [18], that may challenge the current pursuit for generalized insight on the dynamic sensitivities of the bistable structural dynamics due to the combined excitation. By this model formulation, the motions of the cantilever $\underline{x}$ are those directly related to the most prominent dynamic behaviors whether pre- ($p < 1$) or post-buckled ($p > 1$). The equality for the load parameter $p=1$ corresponds to the system loaded at the *elastic stability limit* by magnetic forces that cancel the linear elastic restoring forces [17]; although this latter case is readily investigated by the model formulation developed here, it is not a particular focus of the current study. Although established around a reduced-order framework of investigation, the construction of Eq. (1) and the analytical steps that follow serve as guidance for future research that may consider the multimode (multistable) behavior of other archetypal, post-buckled structures, such as the many modes of buckling in beams and shells to be used for structural or energy harvesting applications [8,39].

Eq. (1) is nondimensionalized to reduce the number of free parameters

$$x'' + \eta x' + (1-p)x + \beta x^3 = -z'' \tag{2}$$

where $x = \underline{x}/l_x$ is a nondimensional displacement with respect to a given characteristic length l_x (for instance, the cantilever length L); $z = \underline{z}/l_x$; $\omega_0 = \sqrt{k_1/m}$ is the natural frequency corresponding to $p=0$, and leads to a normalized pre-buckled natural frequency of $\omega_n = \sqrt{1-p}$ and post-buckled natural frequency $\omega_n = \sqrt{2|1-p|}$; $\tau = \omega_0 t$ is a nondimensional time where its derivative is expressed using $\partial/\partial\tau = (\,)'$; $\beta = k_3 l_x^2/k_1$ is a nondimensional nonlinear stiffness; and the damping loss factor is $\eta = b/m\omega_0$. The excitation includes harmonic and stochastic components

$$-z'' = F\cos\omega\tau + \sigma w(\tau) \tag{3}$$

such that $w(\tau)$ is a Gaussian white noise process with

$$\langle w(\tau)\rangle = 0 \text{ and } \langle w(\tau)w(\tau+\tau_0)\rangle = \delta(\tau_0) \tag{4}$$

and where σ is the standard deviation of the noise [40]. Considering the harmonic excitation component, F is a normalized base acceleration amplitude and ω is the absolute frequency normalized with respect to ω_0.

2.3. Analytical strategy for approximate governing equation solution

To arrive at an analytical prediction for the primary beam oscillations in consequence to the combined excitation, it is assumed that a new, linear governing equation may be used to approximate the various nonlinear dependencies of Eq. (2). This equivalent, linear system is governed by

$$x'' + \eta x' + \omega_e^2 x + \gamma = -z'' \tag{5}$$

where the parameters ω_e^2 and γ are an equivalent linear natural frequency and displacement offset, respectively. These parameters are determined by minimizing the mean-square error between Eqs. (2) and (5). The error is

$$E = (1-p)x + \beta x^3 - \omega_e^2 x - \gamma \tag{6}$$

Minimizing the mean-square of Eq. (6) according to the unknowns ω_e^2 and γ is achieved by simultaneously solving $\partial\langle E^2\rangle/\partial\omega_e^2 = 0$ and $\partial\langle E^2\rangle/\partial\gamma = 0$ [40]. Before this procedure, it is assumed that the total dynamic response for the system governed by Eq. (5) is a superposition of responses individually attributed to the harmonic or stochastic inputs:

$$x(\tau) = x_h(\tau) + x_r(\tau) \tag{7}$$

where x_h is the harmonic component and x_r is the zero-mean component induced by the white noise, i.e. $\langle x_r\rangle = 0$. Moreover, the harmonic component, which accounts for the 'steady-state' contribution to the total response, is expanded via

$$x_h(\tau) = k(\tau) + h(\tau)\sin\omega\tau + g(\tau)\cos\omega\tau = k(\tau) + n(\tau)\cos\left[\omega\tau - \phi(\tau)\right] \tag{8}$$

where the coefficients k, h, and g vary slowly in time, and $n^2 = h^2 + g^2$ and $\tan\phi = h/g$. Using these assumptions, minimizing the mean-square error between Eqs. (2) and (5) is achieved by

$$\frac{\partial\langle E^2\rangle}{\partial\omega_e^2} = \left\langle (1-p)x^2 - \omega_e^2 x^2 + \beta x^4 - \gamma x\right\rangle = 0 \tag{9a}$$

$$\frac{\partial\langle E^2\rangle}{\partial\gamma} = \left\langle (1-p)x - \omega_e^2 x + \beta x^3 - \gamma\right\rangle = 0 \tag{9b}$$

Substitution of the assumed solution Eq. (7) into Eq. (9) enables the determination of ω_e^2 and γ. In advance of this procedure, properties associated with the Gaussian white noise process are assumed, namely that the expectations of the lower-order moments are [41]

$$E[x_r] = \langle x_r \rangle = 0;\ E\left[x_r^2\right] = \left\langle x_r^2 \right\rangle;\ E\left[x_r^3\right] = \left\langle x_r^3 \right\rangle \approx 3\langle x_r \rangle \left\langle x_r^2 \right\rangle - 2\langle x_r \rangle^3;\ E\left[x_r^4\right] = \left\langle x_r^4 \right\rangle \approx 3\left\langle x_r^2 \right\rangle^2 - 2\langle x_r \rangle^4 \tag{10}$$

By this approach, Eq. (9) is solved to yield

$$\omega_e^2 = (1-p) + \frac{3}{4}\beta \frac{n^4 + 8n^2\left\langle x_r^2 \right\rangle + 8\left\langle x_r^2 \right\rangle^2 + 4k^2\left(n^2 + 2\left\langle x_r^2 \right\rangle\right)}{n^2 + 2\left\langle x_r^2 \right\rangle} \tag{11a}$$

$$\gamma = \frac{1}{4}\beta k \frac{3n^4 - 8k^2\left(n^2 + 2\left\langle x_r^2 \right\rangle\right)}{n^2 + 2\left\langle x_r^2 \right\rangle} \tag{11b}$$

Having determined the natural frequency and displacement bias for the linear system governed by Eq. (5), which is approximately equivalent (in a mean-square sense) to the original nonlinear system governed by Eq. (2) [31], on the basis of linear superposition it is assumed that one may solve individually for the responses to

$$x''_h + \eta x'_h + \omega_e^2 x_h + \gamma = F\ \cos\ \omega\tau \tag{12a}$$

and

$$x''_r + \eta x'_r + \omega_e^2 x_r + \gamma = \sigma w(\tau) \tag{12b}$$

and then add together the responses to predict the total dynamic behavior, in accordance with Eq. (7). One observes this analytical methodology to have analogs to the harmonic [42] and stochastic linearization [43] approaches. Substitution of Eq. (8) into Eq. (12a) yields a system

$$\begin{aligned} -\eta k' &= \omega_e^2 k + \gamma \\ -\eta h' + 2\omega g' &= \left(\omega_e^2 - \omega^2\right)h - \eta\omega g \\ -2\omega h' - \eta g' &= \eta\omega h + \left(\omega_e^2 - \omega^2\right)g + F \end{aligned} \tag{13a,b,c}$$

Assuming that this dynamic response reaches steady-state, one finds that $k^2 = 0$ or that $k^2 = \gamma^2/\omega_e^4 = -\frac{3}{2}n^2 - 3\left\langle x_r^2 \right\rangle - (1-p)/\beta$. The non-zero k^2 would correspond to the asymmetric oscillation of the post-buckled beam (respecting an unstable equilibrium at $x = 0$). These results are correspondingly substituted into Eqs. (13b, c) from which one derives

$$n^2 = F^2/\alpha^2 \tag{14}$$

where $\alpha^2 = \left(\omega_e^2 - \omega^2\right)^2 + (\eta\omega)^2$. Eq. (14) gives the squared, harmonic displacement amplitude of the structure as contributed directly from the periodic component of the combined excitation.

Taking the expectation of both sides of Eq. (12b) shows that $\gamma = 0$ for the equivalent stochastic system. Thus, the mean-square displacement resulting from the white noise input into the system given by Eq. (12b) is [31]

$$\left\langle x_r^2 \right\rangle = \frac{\sigma^2}{2\eta\omega_e^2} \tag{15}$$

Concluding, the total, nondimensional, mean-square displacement of the bistable oscillator, considering Eq. (7), is

$$\langle x^2 \rangle = \left\langle x_h^2 \right\rangle + \left\langle x_r^2 \right\rangle = k^2 + \frac{1}{2}n^2 + \left\langle x_r^2 \right\rangle \tag{16}$$

Collectively, Eqs. (11a), (14), and (15) form a set that may be solved using straightforward numerical procedures to predict the harmonic displacement amplitude n, total mean-square displacement $\langle x^2 \rangle$, and equivalent linear natural frequency ω_e of the post-buckled structure response in consequence to the combined harmonic and stochastic base acceleration excitation. In this study, the MATLAB software is employed to solve Eqs. (11a), (14), and (15) via the function *fsolve* that is seen to rapidly identify all potential solutions to this equation system when prescribed initial guesses that are within about an order of magnitude to the actual values. Given the unit-based normalization process used to formulate the governing Eqs. (2) and (5), the software has little difficulty in converging when prescribed initial guesses to solve the equation system are random perturbations away from a unit-valued set. In all results presented hereafter, only stable predictions determined from the solution procedure are retained and presented as the analytical data below. Stability is determined from the Jacobian matrix provided by the numerical solution procedure to Eqs. (11a), (14), and (15): negative real eigenvalues of the Jacobian matrix indicate a stable response. In addition, in the following studies the focus is on cases for which the normalized harmonic excitation frequency ω is within an order of magnitude of the linear natural frequency, which is $\sqrt{2}$ according to the scaling. This focus is based on the prior understanding that the dynamics of bistable structures are most sensitive when driven by harmonic excitations at a frequency near resonance [1,7].

2.4. Simulation of the total dynamic response

Although experimental studies complement the analytical investigations to validate the theoretical formulation developed in this research, direct numerical simulation of the governing equation of motion, Eq. (2), by a brute-force, fourth-order Runge-Kutta method is carried out using rigorous tolerances of error control to best capture the intricacies of stochastic processes. The simulation results assess the efficacy of the model assumptions and formulation, particularly the concept of linear superposition of two behaviors to find an equivalent dynamic response that represents a significantly more complex nonlinear behavior. In all numerical results shown, the responses are determined by 52 individual simulations of Eq. (2) each using randomly-selected initial conditions and a time series lasting 100 periods of motion, respecting the given harmonic excitation term. In the following plots, the 52 simulation results for each parameter as well as their mean values over the 52 initial condition cases are presented. The use of a large number of simulations, each accounting for different initial conditions, ensures that the numerical results are statistically significant given the inclusion of stochastic processes in the investigations.

3. Experimental methods

The experimental system shown in Fig. 1(a) is examined in the laboratory by the following procedures. The absolute cantilever tip bending displacement is measured by a Micro Epsilon ILD-1700 laser sensor. A Micro Epsilon ILD-2300 laser measures the displacement of the electrodynamic shaker table while a collocated accelerometer (PCB Piezotronics 352C33) measures the shaker table acceleration in the same axis of motion. The shaker (LabWorks ET-140) is controlled by a LabVIEW (National Instruments) interface, through an amplifier (LabWorks PA-141), to provide constant-amplitude acceleration at all frequencies considered in the experiments, while the addition of noise is controlled by prescribing the variance of an additive, normally-distributed time series of voltage that superimposes with harmonic voltage that drives the shaker. By this approach, the stochastic contribution to the acceleration excitation may be determined conclusively, from which the stochastic acceleration variance may be computed. Once the data is acquired, all channels are digitally filtered with a low-pass filter at 200 Hz. Lastly, the cantilever tip relative displacement is computed as the difference between the beam absolute displacement subtracted from the shaker absolute displacement.

4. Results and discussions

In the following paragraphs, the analytical and experimental results are presented and discussed, wherein the roles of combined harmonic and stochastic excitation on the sensitivities of dynamic state transitions in the bistable structure are identified and discussed.

4.1. Impact of post-buckling load magnitude and harmonic excitation frequency

For the analytical investigations, the bistable structure damping factor and nonlinear stiffness parameter are unchanged to minimize the number of freely-changed variables. The values of these variables are, respectively, $\eta=0.02$ and $\beta=0.1$. The damping factor η is in accordance with the measurements of the loss factor in the experimental system, while the nonlinearity term β is selected based on the small amplitudes of oscillation observed, with respect to the beam length.

The top row of Fig. 2 presents analytical predictions of the normalized harmonic displacement amplitude n for a harmonic excitation amplitude $F=0.15$ across a range of normalized excitation frequencies $0.2 \leq \omega \leq 2$ known to yield more intricate and relevant dynamic behaviors for linear and nonlinear structures [16]. The columns, from left to right, show analytical predictions for increasing values of the load parameter $p = \left[1.5, 2.0, 2.6\right]$; these values correspond to post-buckled configurations of the beam, with increasing parameter values indicating larger distances between the two stable equilibria and normalized natural frequencies, respectively, of 1.0, 1.4, and 1.8. The dash-dot (dashed) curves correspond to asymmetric (symmetric) displacement responses in the absence of stochastic contributions to the excitation, $\sigma=0$. Such behaviors are the well-known, steady-state dynamic response regimes of post-buckled structures [1] characterized respectively as either oscillations around one local equilibria (intrawell) or as large amplitude, snap-through vibrations that cross between the two stable equilibria (interwell). In the experimental system, the unstable equilibrium configuration corresponds to the beam pointed between the magnet pair, in other words in between the two stable equilibria. Despite the possible 'coexistence' of response behaviors shown in Fig. 2, practically only one such steady-state may exist at any given moment in time [19], and initial conditions and perturbations to the system may change the instantaneous dynamic regime [44]. The top row of Fig. 3 presents the measurements from the experimental system that are found to closely correspond to the influences observed through the analysis, with symmetric (asymmetric) responses indicated by the unfilled circle (diamond) data points. To obtain the measurements, the harmonic acceleration amplitude of 0.75 m/s^2 is held constant while the frequency is slowly swept at a rate of 0.08 Hz/s in increasing and then decreasing increments; then, fast Fourier transforms are computed over the time series to obtain the individual data points. The supplementary video 1 for this research gives plain visual evidence of the steady-state dynamics of the symmetric post-buckled beam. Comparing the

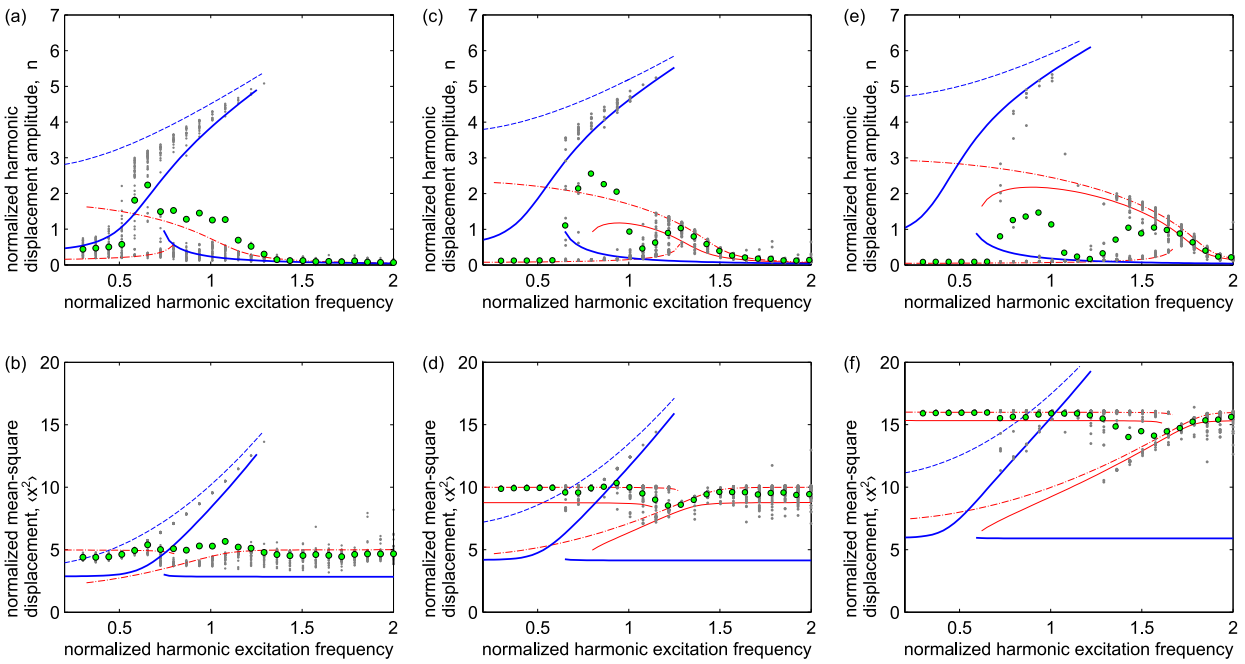

Fig. 2. Analytical predictions of the beam normalized harmonic displacement amplitude (a, c, e), and normalized mean-square displacement (b, d, f) with harmonic excitation amplitude $F=0.15$. Dashed (dash-dot) curves indicate symmetric (asymmetric) response without stochastic excitation, $\sigma=0$. Thick blue (thin red) solid curves indicate symmetric (asymmetric) response with noise $\sigma=0.20=4$ F/3. Dots and filled circles are, respectively, the individual and means results of 52 numerical simulations conducted at each excitation frequency. The first column presents results for load parameter $p=1.5$, the second column for $p=2.0$, and third column for $p=2.6$. The corresponding normalized natural frequencies are $\omega_n=1.0$, 1.4, and 1.8, respectively. (For interpretation of the references to color in this figure legend, the reader is referred to the web version of this article).

displacement amplitudes predicted for the purely harmonic excitation, it is seen that the influence of changing load parameter from low to high values of p and when using greater magnet spacing distances Δ (for the range herein considered) lead to several distinguishing shifts in the occurrence of the coexisting, steady-state dynamics that are corroborated between analysis and experiment. Namely, as these respective parameters increase: (i) the intrawell dynamic regime, shown as dash-dot curves in Fig. 2 and as light red diamonds in Fig. 3, exhibits a progressively increasing linear natural frequency; (ii) the frequency range across which two, different amplitudes of this intrawell response is seen to broaden; and (iii) the large, amplitude snap-through oscillation, shown as dashed curves in Fig. 2 and as dark blue circles in Fig. 3, is diminished in its peak frequency of occurrence while the amplitudes of snap-through displacement are magnified across all frequencies that it may be activated. In each of these ways, the analytical trends have supporting analogs in the experimental findings.

Supplementary material related to this article can be found online at http://dx.doi.org/10.1016/j.jsv.2017.02.006.

The second rows of Figs. 2 and 3 present the analytical/numerical and experimental results of the mean-square beam displacement, which, considering the responses subjected only to the harmonic excitation component, consist of values associated with the displacement bias due to intrawell oscillations and due to the harmonic amplitude of motion, Eq. (16). Comparing the first and second rows of these figures reveals that at lower frequencies of the harmonic excitation, the snap-through dynamic regime may lead to smaller mean-square displacements than those occurring for an intrawell dynamic regime. A practical explanation for this effect is that the snap-through motions in lower frequency bandwidths do not significantly overshoot the locations of the two stable equilibria per excitation cycle. Thus, with a zero mean, and considering Eq. (16), snap-through motions must appreciably overshoot the stable equilibria locations in order to possess mean-squares of greater value than a coexistent intrawell oscillation. These trends are in good agreement between the measurements shown in the second row of Fig. 3 and predictions of the bistable structure dynamics in the second row of Fig. 2.

The introduction of the stochastic excitation contribution considerably changes the landscape of the dynamics that the bistable structure undergoes. In the analysis, a white noise with standard deviation $\sigma = 4F/3 = 0.20$ is predicted to uniformly diminish the harmonic displacement amplitudes of the snap-through dynamics, as shown in the top row of Fig. 2 comparing the dashed blue to thick blue solid curves. In addition, the bandwidth of frequencies over which intrawell dynamics are predicted to occur is significantly reduced or entirely suppressed like that result shown in Fig. 2(a) (blue thick curve). These factors of the analytical predictions are in good agreement with the results of the individual numerical simulations (grey points) that can be considered as individual case-study stochastic responses in comparison to the mean numerical result for each frequency (filled circles) that is comparable to a long-time average of the case-study trends. On the other hand, as observed considering Fig. 2 from left to right columns in the bottom row, increasing deviations are seen in the analytically predicted mean-square displacements when compared to simulations as the load parameter p increases, corresponding to

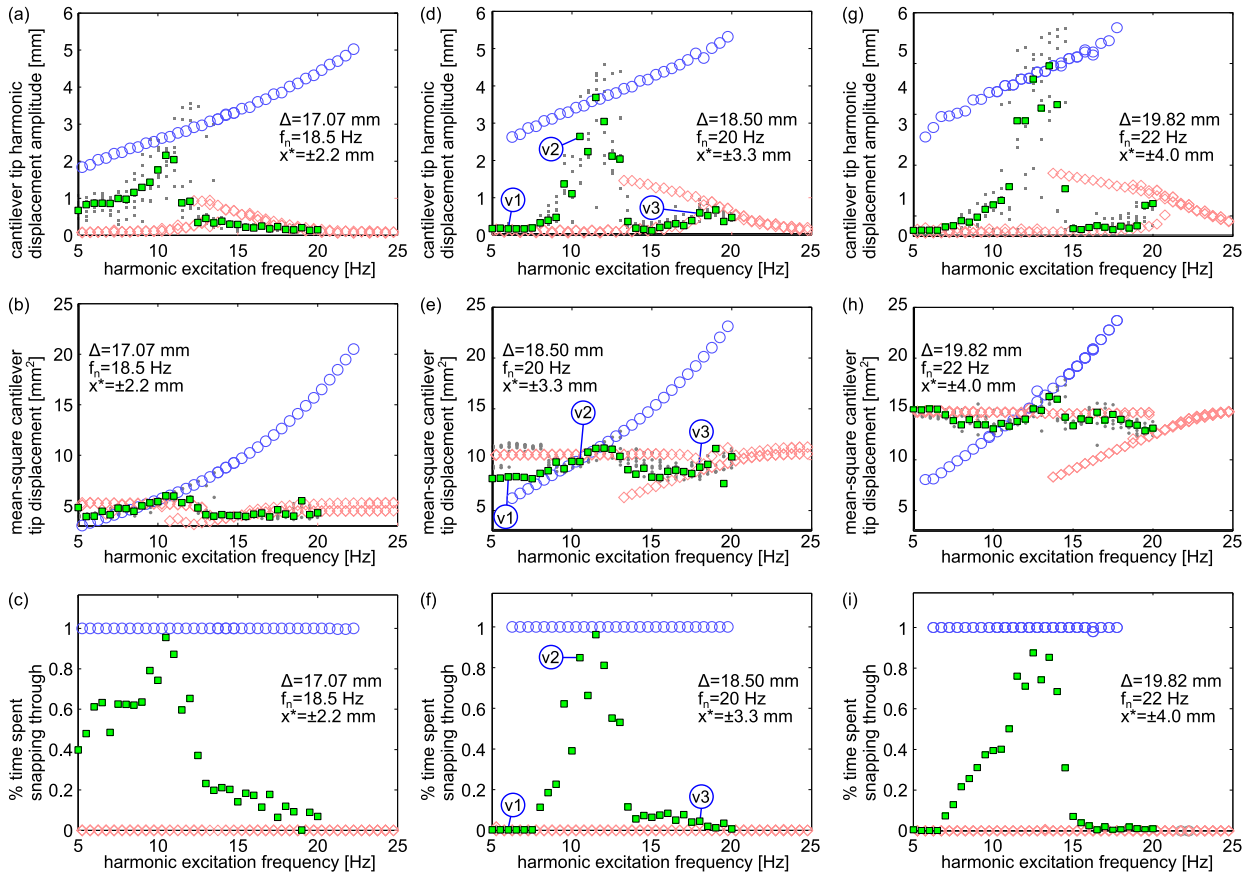

Fig. 3. Experimental measurements of cantilever tip harmonic displacement amplitude (a, d, g), mean-square displacement (b, e, h), and percentage of time that the beam spends snapping through per 30-s stationary excitation (c, f, i) with harmonic excitation acceleration amplitude 0.75 m/s^2. Open circle (closed diamond) data points indicate symmetric (asymmetric) response without stochastic excitation, such that the acceleration standard deviation is 0 m/s^2. Dots and filled circles are, respectively, the short-time and mean evaluations of measurements using the harmonic excitation with an additive base acceleration noise of standard deviation of 1 m/s^2 which is 4/3 of the harmonic amplitude. From left to right columns, an increasing distance between the stable equilibria is induced by increasing the magnet positioning parameter Δ. The values of the parameter Δ, natural frequency, and stable equilibria positions are, respectively, for the first column 17.07 mm, 18.5 Hz, $\pm$2.2 mm; for the second column 18.50 mm, 20 Hz, $\pm$3.3 mm; for the third column 19.82 mm, 22 Hz, $\pm$4.0 mm.

greater distance between the stable equilibria (since the nonlinearity term β is constant). This reflects the limitation of stochastic linearization procedures to accurately predict statistical measures of dynamic response for post-buckled structures for cases involving closely-spaced stable equilibria spanned by small energetic barriers [45], which is progressively challenged by the increase in load parameter p.

The experimental measurements of the magnetoelastic, post-buckled beam when excited with an acceleration amplitude of 0.75 m/s^2 and additive noise with standard deviation 1 m/s^2 (filled squares) agree well with the findings from the model; note that the standard deviation of the stochastic excitation employed in the experiment is of the same proportion to the harmonic component as that included in the analytical results of Fig. 2. For each measured data point in Fig. 3 that considers such combined harmonic and stochastic excitation (filled squares), the respective result is computed from a 30 s-long dwell at the frequency of the harmonic excitation, and thus is comparable to the numerical long-time average results (filled circles) shown as validation for the analytical results in Fig. 2. Shown as grey points in the background of the first and second rows of Fig. 3 are samples of the displacement amplitude and mean-square displacement computed from short-time (6-s duration) evaluations of the 30 s-long dwell, which are thus comparable to the individual numerical simulation results of Fig. 2 that are shown as grey points.

Using the data points featured with the labels in Fig. 3(d, e, f), the experimental results reveal practical nuances of the dynamic behaviors observed under the combined harmonic and stochastic excitations, and guide one towards insights on the dynamic sensitivities. Fig. 4(a) shows portions of the displacement time series for the points labeled as v1, v2, and v3 in Fig. 3(d, e, f). Using the phase-lag-based phase portrait [1] where T as the harmonic excitation period, the characteristics of the trajectories are plainly assessed. For example, due to the consolidation of the oscillations to a small region in Fig. 4(a), the trajectory v1 is an intrawell behavior that responds so negligibly at the harmonic excitation frequency that the beam is more effectively driven by the noise excitation component to respond at the fundamental natural frequency around 20 Hz

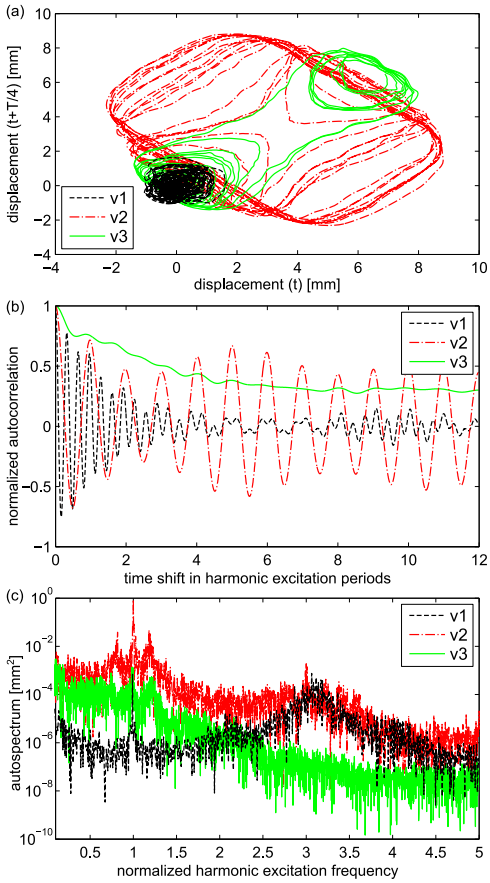

Fig. 4. Portions of time series recordings of beam displacement as indicated by the labels v1, v2, and v3 in Fig. 3(d, e, f). Here, (a) shows a phase-lag phase portrait of the beam displacement response for a portion of this time series span, (b) shows the autocorrelation of the corresponding data point, and (c) shows the autospectrum of the corresponding data point.

(or around 3.2 times the harmonic excitation frequency). This observation is evident in the corresponding autocorrelation and autospectrum plots Fig. 4(b) and (c). In contrast, the trajectory v2 in Fig. 4 reveals a snap-through dynamic of large displacement and phase-lagged displacement, and more appreciable autocorrelation of the system response when shifted by integer multiples of the excitation period. Yet, the noise still contributes so greatly to this total response that the oscillation exhibits a rapidly fading 'memory' as shown in the decaying autocorrelation values as the time shift increases, Fig. 4 (b). Interestingly, the autocorrelation also reveals a modulating envelope trend, with peaks around $5i$ excitation periods' worth of delay where $i = 1, 2, ...$, which could be the sign of a time-dependent dynamic sensitivity for the snap-through response. Finally, the trajectory v3 in Fig. 4 exhibits only occasional snap-through oscillations between the two stable equilibria, resulting in an autocorrelation trend with a fading non-zero bias, in contrast to the sinusoidal-like characteristics more often attributed to the autocorrelation of periodic dynamics. Key characteristics of these results, shown by time series, are evident in the supplementary video 2 where the dynamics of the post-buckled beam are shown when the system is subjected to different combinations of harmonic and stochastic excitations.

Supplementary material related to this article can be found online at http://dx.doi.org/10.1016/j.jsv.2017.02.006.

Considering the v2 and v3 trajectories in Fig. 4 and the corresponding results of Fig. 3(f) that present the percentage of time the beam spends snapping through per 30 s-long constant-frequency dwell, it appears that the coexistent snap-through dynamic near the beam natural frequency of 20 Hz, when the noise is absent, is effectively disabled by the additive noise. This conclusion is strongly supported by the corresponding short-time evaluations in Fig. 3(d) and (e) in the frequency range close to the natural frequency of 20 Hz, which exhibit values very close to those that are computed for the asymmetric, intrawell oscillation regime in the absence of noise. On the other hand, the snap-through motions occurring at frequencies around 50–60% of the natural frequency are readily promoted by the introduction of the noise since the percentage of time spent snapping through is large around these frequencies, such as for the v2 trajectory in Fig. 3(f) and as evident in the short-time data evaluations in Fig. 3(d). These trends are also observed via Fig. 3(c, i) according to the respective natural frequencies and proportions thereof obtained for the other cases of magnet positioning parameter Δ. Indeed, the analytical and numerical mean results in the first row of Fig. 2 for all load parameters p likewise reveal significant amplification of the overall harmonic displacement amplitude at frequencies around 50–60% of resonance, while

the harmonic excitation at frequencies closer to resonance is comparatively unable to induce snap-through responses, judging by the significantly smaller amplitudes of the harmonic response and return to intrawell oscillations. Thus, supported by the analytical, numerical, and experimental evidence, structures with bistable members are more susceptible to undergoing dynamic regime transitions when the harmonic excitation component drives the system at a frequency around 50–60% of the natural frequency in the presence of a non-trivial additive white noise excitation.

Further insights may be drawn from the analytical, numerical, and experimental evidence collected in Figs. 2 and 3. For instance, increase in the load parameter (over the range considered here) leads to an increase in the harmonic excitation frequency at which the beam snaps through with greater regularity when subjected to the combined harmonic and stochastic excitation. For example, this is seen in the mean numerical data shown in Fig. 2 by considering the increase in the frequency of the maximum numerical mean value from about 0.65 to 0.80 to 0.94 as the load parameter p increases from 1.5 to 2.0 to 2.6 spanning, respectively, from Fig. 2(a) to (d) to (g). Similarly, as the magnet positioning parameter Δ increases from 17.07 to 18.50 to 19.82 mm, Fig. 3(a, d, g), the frequency of maximum beam displacement amplitude in consequence to the combined harmonic and stochastic excitation increases from about 10 to 12 to 14 Hz. These experimental trends are plainly revealed through the time percentages of snap-through response, as shown in the bottom row of Fig. 3. Because the increase in load and magnet positioning parameters correspond to increase in the linear natural frequency of each system configuration, seen according to the inset labels and spectral locations of the 'softening' intrawell resonant responses, it is apparent that when under stochastic and harmonic excitations the frequency of greatest sensitivity to induce transitions among the coexisting dynamic regimes is related to the linear natural frequency. This supplemental observation supports the finding described in the preceding paragraph, and connects it to the variation of load or magnetic positioning parameters that are representative of the extent of post-buckling, whether severely post-buckled with very high natural frequency or vice-versa [16].

How may the analytical method and results predict such sensitive conditions for the bistable structure response, thereby providing designers insight on operational parameters that could induce transitions among the dynamic regimes? Reflecting upon the results of Figs. 2 and 3, it is observed that an important trend rests in the mean numerical results and the experimental results of the mean-square beam displacement. First, it is recognized that the squared stable equilibria distance k^2 (measured from the unstable equilibrium) is the mean-square beam displacement at very high or very low frequencies when noise is absent, since the amplitude of the harmonic response is negligible, according to Eq. (16). As a result, the squared stable equilibria distance is equivalently shown at very high or very low frequencies by the noise-free analytical predictions for the intrawell regime with the dash-dot curve in the second row of Fig. 2, and by the noise-free measurements shown by the light circles in the second row of Fig. 3. This in mind, it is observed from the numerical and measured data that the values of the mean numerical results and the experimental results of the mean-square beam displacement are equal to or exceed the squared stable equilibria distance at approximately the frequency that promotes the greatest amplitude of beam displacement and thus the greatest percentage of time snapping through. According to the analytical model expressions, this observation is equivalent to

$$\frac{1}{2}n^2 + \frac{\sigma^2}{2\eta\omega_e^2} + \frac{1-p}{\beta} = 0 \tag{17}$$

The relationship in Eq. (17) is recursive because $n = f(\omega_e)$, $\omega_e = f\left(n, \left\langle x_r^2 \right\rangle\right)$, and $\left\langle x_r^2 \right\rangle = f(\omega_e)$. By substitution of Eq. (15) into (11a), an expression $0 = \omega_e(n)$ is obtained. Since this latter expression is equal to zero, and considering the equality of Eq. (17), one may plot the transcendental functions such that Eq. (17) is equal to $\omega_e(n)$, for instance as a function of the n values obtained from the analytical model. The intersection of the curves is the value of n resulting from harmonic excitation at the frequency at which the beam spends the greatest percentage of time snapping through, according to the observation described above. Then, by Eq. (17), $\omega_e^2 = -\beta\sigma^2/\left[\eta\left(2(1-p)+\beta n^2\right)\right]$. Thereafter, one may solve Eq. (14) for a first approximation of the frequency at which the beam snaps through the most regularly due to the combined harmonic and stochastic loading,

$$\omega = \left[\omega_e^2 - \frac{1}{2}\eta^2 \pm \frac{1}{2n}\left(4F^2 - 4\eta^2 n^2\omega_e^2 + \eta^4 n^2\right)^{1/2}\right]^{1/2} \tag{18}$$

Using this framework, consider again the analytically predicted results shown in Fig. 2. For $p=1.5$, resolving the transcendental function identifies 2.51 as the value of n where this occurs. Then, according to Eq. (18), the harmonic excitation frequency which most promotes the snap-through dynamic under the additional contribution of the stochastic excitation is $\omega = [0.69, 0.77]$. Repeating this routine for the load parameters $p=2.0$ and 2.6, respectively, yield $\omega = [0.88, 0.92]$ and $\omega = [1.02, 1.04]$. These predictions compare well against the numerical results that reveal peak occurrences of snap-through behaviors around $\omega=0.65$, $\omega=0.80$, and $\omega=0.94$, respectively, for $p=1.5$, 2.0, and 2.6. For a first approximation, the analytical predictions of the model and ensuing implementation of Eq. (18) are useful tools for the design and implementation of post-buckled structures under such complex, combined excitations to ensure that the dynamic regime of interest is sustained.

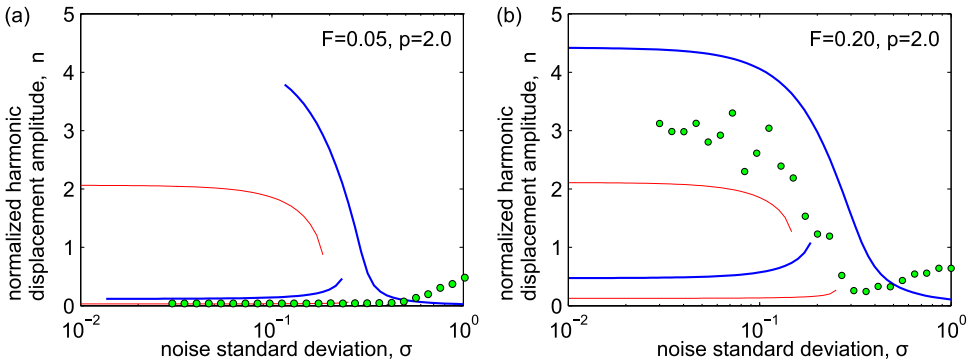

Fig. 5. Analytical predictions of the beam normalized harmonic displacement amplitude. Thick blue (thin red) solid curves indicate symmetric (asymmetric) response with varying noise standard deviation σ. Filled circles are the means results of 52 numerical simulations conducted for each noise standard deviation. (a) Presents results for harmonic excitation amplitude of $F=0.05$ and (b) $F=0.20$. The normalized harmonic excitation frequency is $\omega=0.65$. (For interpretation of the references to color in this figure legend, the reader is referred to the web version of this article).

4.2. Influences of stochastic excitation standard deviation to the steady-state dynamic response

Previous investigators have studied the roles of stochastic excitation on the dynamics of bistable structures that are also driven by a harmonic excitation component with emphasis on characterizing the phenomenon known as stochastic resonance [46–49]. This intriguing behavior promotes an interwell response when the bistable system is excited by (I) stochastic loads with (II) a small harmonic loading mechanism oftentimes parametric in effect [47,49]. Despite the low levels of the harmonic loading, the interwell dynamic becomes synchronized with the harmonic period of this excitation component. Recently, stochastic resonance was numerically and experimentally observed in a study on a thermally-buckled and base-excited beam [44] giving new evidence of this phenomenon's existence in practical, imperfect structures. In contrast to the extensive numerical and experimental investigations focused on the intriguing phenomenon, this research is more concerned with elucidating the overall dynamic sensitivities exhibited by post-buckled structures under combined harmonic and stochastic excitation mechanisms, whether or not associated with stochastic resonance, and focused on establishing an experimentally-validated, analytical tool that might predict such influences. Thus, this section applies the new analytical method and experimental evidence to uncover the intricate roles of change in stochastic loads upon the archetypal bistable structure dynamics.

Using thick (thin) curves, Fig. 5 plots analytical predictions of the symmetric (asymmetric) harmonic displacement amplitudes when the harmonic excitation has level (a) $F=0.05$ and (b) $F=0.20$ while the standard deviation of the noise σ is varied across two orders of magnitude. For these results, the load parameter is $p=2.0$ and the frequency of the harmonic excitation is $\omega=0.65$ which is close to the sensitive bandwidth for inducing state transition as indicated above. Fig. 6 (a) presents a comparable data set measured experimentally when the ferromagnetic cantilever has a magnet positioning parameter $\Delta=17.66$ mm, considering the circle and triangle data points that, respectively, present the cantilever tip harmonic displacement amplitudes for a harmonic level of the base acceleration of 0.69 and 1.58 m/s^2. Here, the standard deviation of the stochastic base acceleration component is varied across about two orders of magnitude while the harmonic frequency of excitation remains at 12 Hz, which is 63% of the linear natural frequency (19 Hz). Similar to the relation between model results of Fig. 2 and measurements of Fig. 3, the data plotted in Fig. 6(a) are comparable to the numerical mean values shown in Fig. 5 (filled circles). For ease of presentation, the short-time data evaluations are omitted from Fig. 6.

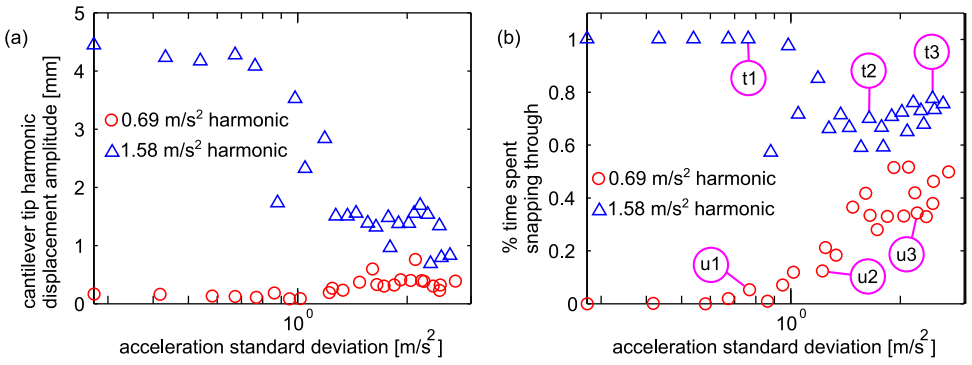

Fig. 6. Experimental measurements of (a) cantilever tip harmonic displacement amplitude and (b) percentage of time that the beam spends snapping through per 30-s stationary excitation as a function of variation in the base acceleration standard deviation for two levels of harmonic acceleration. The harmonic excitation frequency is 12 Hz, and the magnet positioning parameter is $\Delta=17.66$ mm.

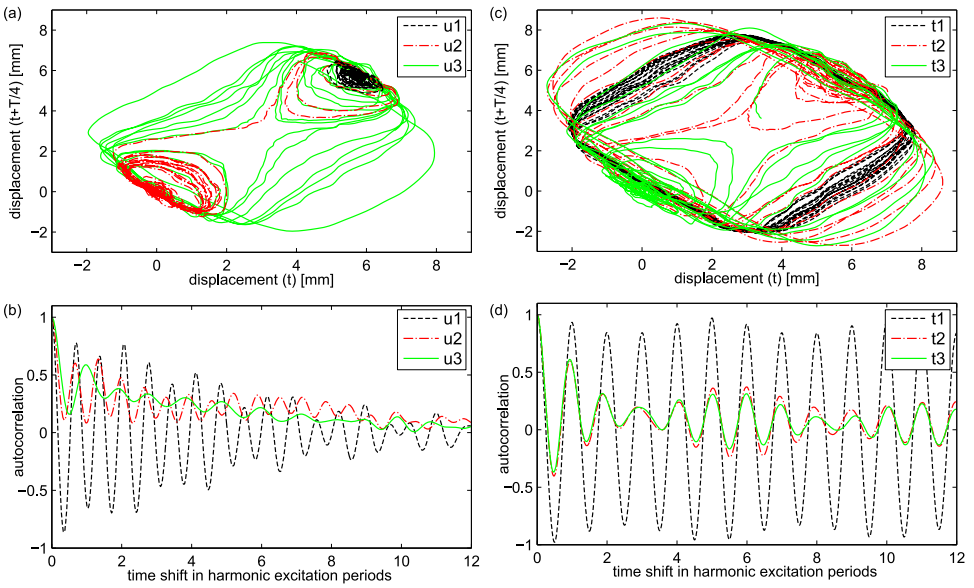

Fig. 7. Portions of time series recordings of beam displacement as indicated by the labels (a, b) u1, u2, and u3, and (c, d) t1, t2, and t3, from Fig. 6(b). Here, (a, c) show phase-lag phase portraits of the beam displacement response for a portion of this time series spans, while (b, d) show the autocorrelation of the corresponding data points.

For the lowest level of harmonic excitation, $F=0.05$, the analytical predictions indicate that standard deviations of the noise notably greater than the harmonic component may activate transitions from the 'steady-state' asymmetric intrawell dynamic regime to the large amplitude, symmetric snap-through response. Specifically, the large amplitude, symmetric response, only occurs once the noise standard deviation is about $\sigma > 2F=0.1$. The numerical mean results in Fig. 5(a) support this analytical trend according to the consistently low amplitudes of the harmonic structure response at the excitation frequency until the values of σ increase considerably beyond the harmonic amplitude F. Experimentally, these themes are observed for the case of the harmonic base acceleration of 0.69 m/s^2 presented by the circle data points in Fig. 6(a) and (b): a low amplitude intrawell response is induced to undergo steady-state regime transitions once the standard deviation of the noise increases substantially enough. Focusing on this case of lower harmonic base acceleration, Fig. 7(a) and (b) respectively plot portions of the phase-lag-based phase portrait and autocorrelation for the data points labeled as u1, u2, and u3 in Fig. 6(b). When the standard deviation of the stochastic excitation is low, the dashed curve for trajectory u1 exemplifies that the response is local to periodic motions around one stable equilibrium. These intrawell oscillations primarily occur at the linear natural frequency instead of the frequency of the harmonic excitation, due to the autocorrelation time shift periodicity of about 0.64 of the 12 Hz excitation natural period, indicating principal response around 18.75 Hz which is close to the 19 Hz natural frequency. As the stochastic amplitude increases, the u2 trajectory indicates that occasional transitions among the different dynamic regimes may occur, causing large fluctuations in overall structural configuration due to a sudden shift in the displacement bias of the bistable system. As the standard deviation of the noise increases still further, the u3 trajectory (solid curve) in Fig. 7(a) reveals that a greater regularity in the transitions among steady states is realized. Importantly, the autocorrelation in Fig. 7(b) indicates that the periodicity of these motions is now at the harmonic excitation frequency, despite the fading bias associated with imperfect persistence of the snap-through behavior. In other words, the increase in noise level causes a change in the dynamic response from a mostly stochastic oscillation at the linear natural frequency, to a dynamic behavior closely synchronized with the very low level of the harmonic excitation component; this is plainly an experimental observation of stochastic resonance, like that reported recently for the thermally buckled, clamped beam [44]. Experimentally, the increase in the percentage of time that the beam spends snapping through is observed for standard deviations of noise around 1.3 m/s^2 and greater, which is approximately twice the harmonic amplitude of the excitation. Indeed, this experimental result agrees with the analytically predicted onset of the snap-through regime in Fig. 5(a) that occurs once $\sigma > 2F=0.1$. As a result, the good agreement between the trends of experiment for the low level of harmonic base acceleration of 0.69 m/s^2 and the analytical results in Fig. 5(a) for $F=0.05$ suggest that the new analytical methods can assist in the prediction of stochastic resonance-based effects and enable designers to either work with or against these phenomena more directly in application.

An alternative influence of the additive white noise excitation is exemplified in the model results shown in Fig. 5(b) and the experimental measurements shown as triangle data points in Fig. 6(a) and (b). Here, the snap-through response regime is persistent when the standard deviation of the stochastic excitation contribution is small, because the harmonic amplitude of the single-frequency excitation is great enough to sustain such large amplitude displacement response. In this case, the mean numerical values shown in Fig. 5(b) confirm that the amplitude of the harmonic displacements are near to the analytically predicted values of the symmetric, snap-through dynamics, while the experimental measurements in Fig. 6

(b) reveal a near-perfect persistence of snap-through oscillations per excitation cycle for small acceleration standard deviation. The trajectory t1, labeled in Fig. 6(b) and elaborated on with the presentations in Fig. 7(c) and (d), exemplifies such consistent vibration, with very little 'memory loss' evident in the autocorrelation envelope as the time shift increases and a phase portrait that is mostly consolidated. The analytical predictions in Fig. 5(b) show that the amplitude of the bistable structure response associated with the harmonic excitation is reduced as the stochastic component becomes more appreciable, such as around $\sigma \approx$ 0.1. Thereafter, the symmetric dynamic is greatly suppressed in amplitude, as verified by the corresponding mean of the numerical simulations. Likewise, the experimental measurements in Fig. 6(a) show that the amplitude of the harmonic displacement of the cantilever reduce progressively starting around the increase of base acceleration standard deviation to about 0.9 m/s^2 and greater. Thus, the analytically predicted proportion of stochastic to harmonic excitations to induce the transition from snap-through regime to a loss of such persistence is around 1:2, while the corresponding experimental measurements result observe the same influence for the proportionality of about 1:1.76. The good agreement between the analytically predicted proportion and the measured result indicate the theoretical formulation established here can be leveraged for future design and implementation of post-buckled structures where the robustness of such constituents are critical to elucidate for effective functioning. In fact, even though the persistence of the snap-through oscillation is compromised as the standard deviation of the excitation is increased beyond this key ratio, the experimental trajectories t2 and t3 show that the periodicity of the oscillations are still consolidated to the same period as the harmonic excitation component. The autocorrelation computations in Fig. 7(d) for t2 and t3 indicate a strongly fading memory, but one that nevertheless repeats mostly in the same period as the harmonic excitation component.

From these findings, and considering the sensitive case that the harmonic excitation is at about 60–65% of the natural frequency, one may conclude that the dynamic stability of snap-through response is more vulnerable to the stochastic excitation contribution when the standard deviation of the base acceleration is approximately one-half of the harmonic component. In contrast, for post-buckled structures undergoing small amplitude intrawell oscillations due to a low level of harmonic excitation, stochastic resonance-like phenomena may occur if the driving noise standard deviation approaches or exceeds twice the amplitude of the harmonic component. Such a quantification of the robustness and susceptibilities of post-buckled structures is newly enabled through the combined analytical, numerical, and experimental methods, tools, and evidence created and assessed in this research. These developments and discoveries also complement prior efforts to illuminate stochastic resonance phenomena via computational and experimental approaches in myriad science and engineering applications [44,46–49], by a new broader theoretical perspective that elucidates the range of dynamic behaviors in post-buckled structures from conventional harmonic response to purely stochastic process.

5. Conclusions

Robust performance and functionality are demanded in many modern engineering applications. The multiplying interests and relevance of post-buckled, bistable members in diverse engineering contexts warrants their close study and attention in order to characterize the sensitivities of the various dynamic regimes unique to these platforms, such as the small amplitude intrawell oscillations around local stable equilibrium configurations and the large amplitude snap-through response corresponding to significant displacements and kinetic energy. While previous studies have numerically and experimentally shown that the presence of stochastic contributions to a total excitation on bistable structures may change the resulting steady-state response regime, this research formulates a new analytical tool for the direct prediction of such critical susceptibilities. Through comprehensive analytical, numerical, and experimental studies on the influences of combined harmonic and stochastic excitations, it is found that the intrawell oscillation regime becomes significantly less sustainable when the excitation frequency of the harmonic excitation component is around 60–65% of the system's natural frequency. Comparatively, the snap-through response is effectively disabled by the stochastic excitation if the harmonic excitation frequency is close to the natural frequency. The loss of the robustness of these dynamic regimes extends to the variation in the stochastic excitation standard deviation, and may be characterized according to key proportionalities of the noise standard deviation and the amplitude of the harmonic excitation. All together, this research establishes a new pathway forward to design and implement post-buckled structures in applications where reliability in performance and effectiveness are demanded.

Acknowledgements

R.L.H. acknowledges start-up funds from the Department of Mechanical and Aerospace Engineering at The Ohio State University (OSU). Q.D. acknowledges support from the OSU College of Engineering Honors Research Scholarship.

References

[1] L.N. Virgin, *Introduction to Experimental Nonlinear Dynamics*, Cambridge University Press, Cambridge, 2000.
[2] C.R. McInnes, D.G. Gorman, M.P. Cartmell, Enhanced vibrational energy harvesting using nonlinear stochastic resonance, *J. Sound Vib.* 318 (2008)

655–662.
[3] S. Zhao, A. Erturk, On the stochastic excitation of monostable and bistable electroelastic power generators: relative advantages and tradeoffs in a physical system, *Appl. Phys. Lett.* 102 (2013) 103902.
[4] R.L. Harne, K.W. Wang, Prospects for nonlinear energy harvesting systems designed near the elastic stability limit when driven by colored noise, *ASME J. Vib. Acoust.* 136 (2014) 021009.
[5] P. Wang, F. Casadei, S. Shan, J.C. Weaver, K. Bertoldi, Harnessing buckling to design tunable locally resonant acoustic metamaterials, *Phys. Rev. Lett.* 113 (2014) 014301.
[6] S. Shan, S.H. Kang, J.R. Raney, P. Wang, L. Fang, F. Candido, J.A. Lewis, K. Bertoldi, Multistable architected materials for trapping elastic strain energy, *Adv. Mater.* 27 (2015) 4296–4301.
[7] N. Kidambi, R.L. Harne, K.W. Wang, Adaptation of energy dissipation in a mechanical metastable module excited near resonance, *J. Vib. Acoust.* 138 (2016) 011001.
[8] N. Hu, R. Burgueño, Elastic postbuckling response of axially-loaded cylindrical shells with seeded geometric imperfection design, *Thin-Walled Struct.* 96 (2015) 256–268.
[9] D. Yang, B. Mosadegh, A. Ainla, B. Lee, F. Khashai, Z. Suo, K. Bertoldi, G.M. Whitesides, Buckling of elastomeric beams enables actuation of soft machines, *Adv. Mater.* 27 (2015) 6323–6327.
[10] N. Hu, R. Burgueño, Buckling-induced smart applications: recent advances and trends, *Smart Mater. Struct.* 24 (2015) 063001.
[11] C.G. Dávila, C. Bisagni, C.A. Rose, Effect of buckling modes on the fatigue life and damage tolerance of stiffened structures, in: Proceedings of the 56th AIAA/ASCE/AHS/ASC Structures, Structural Dynamics, and Materials Conference, AIAA SciTech, Kissimmee, Florida, USA, 2015, pp. AIAA 2015–1436.
[12] P.C. Chen and M.P. Mignolet, Fatigue life of composite structures in extreme environments, Air Force Research Laboratory, Wright Patternson Air Force Base, OH, 2005, pp. AFRL-VA-WP-TR-2005–3065.
[13] S.M. Spottswood, T.G. Eason, X.Q. Wang, M.P. Mignolet, Nonlinear reduced order modeling of curved beams: a comparison of methods, in: Proceedings of the 50th AIAA/ASME/ASCE/AHS/ASC Structures, Structural Dynamics, and Materials Conference, Palm Springs, California, USA, 2009, pp. AIAA 2009–2433.
[14] A.J. Culler, J.J. McNamara, Studies on fluid-thermal-structural coupling for aerothermoelasticity in hypersonic flow, *AIAA J.* 48 (2010) 1721–1738.
[15] B.A. Miller, J.J. McNamara, S.M. Spottswood, A.J. Culler, The impact of flow induced loads on snap-through behavior of acoustically excited, thermally buckled panels, *J. Sound Vib.* 330 (2011) 5736–5752.
[16] L.N. Virgin, *Vibration of Axially Loaded Structures*, Cambridge University Press, Cambridge, 2007.
[17] Z.P. Bažant, L. Cedolin, *Stability of Structures: elastic, Inelastic, Fracture, and Damage Theories*, World Scientific Publishing Co, Hackensack, New Jersey, 2010.
[18] F.C. Moon, P.J. Holmes, A magnetoelastic strange attractor, *J. Sound Vib.* 65 (1979) 275–296.
[19] W. Szemplińska-Stupnicka, J. Rudowski, Steady states in the twin-well potential oscillator: computer simulations and approximate analytical studies, *Chaos* 3 (1993) 375–385.
[20] L.N. Virgin, The dynamics of symmetric post-buckling, *Int. J. Mech. Sci.* 27 (1985) 235–248.
[21] R.L. Harne, M. Thota, K.W. Wang, Concise and high-fidelity predictive criteria for maximizing performance and robustness of bistable energy harvesters, *Appl. Phys. Lett.* 102 (2013) 053903.
[22] M. Panyam, R. Masana, M.F. Daqaq, On approximating the effective bandwidth of bi-stable energy harvesters, *Int. J. Non-Linear Mech.* 67 (2014) 153–163.
[23] M.F. Daqaq, Transduction of a bistable inductive generator driven by white and exponentially correlated Gaussian noise, *J. Sound Vib.* 330 (2011) 2554–2564.
[24] I. Kovacic, M. Cartmell, M. Zukovic, Mixed-mode dynamics of certain bistable oscillators: behavioural mapping, approximations for motion and links with van der Pol oscillators, *Proc. R. Soc. A* 471 (2015) 20150638.
[25] C. Zhang, R.L. Harne, B. Li, K.W. Wang, Reconstructing the transient, dissipative dynamics of a bistable Duffing oscillator with an enhanced averaging method and Jacobian elliptic functions, *Int. J. Non-Linear Mech.* 79 (2016) 26–37.
[26] J.D. Turner, A.J. Pretlove, A study of the spectrum of traffic-induced bridge vibration, *J. Sound Vib.* 122 (1988) 31–42.
[27] P.L. Green, E. Papatheou, N.D. Sims, Energy harvesting from human motion and bridge vibrations: an evaluation of current nonlinear energy harvesting solutions, *J. Intell. Mater. Syst. Struct.* 24 (2013) 1494–1505.
[28] P.W. Bearman, Vortex shedding from oscillating bluff bodies, *Annu. Rev. Fluid Mech.* 16 (1984) 195–222.
[29] S. Corda, R.J. Franz, J.N. Blanton, M.J. Vachon, J.B. DeBoer, In-flight vibration environment of the NASA F-15B flight test fixture, *NASA* (2002). (pp. TM-2002-210719).
[30] A.T. Wall, K.L. Gee, M.M. James, K.A. Bradley, S.A. McInerny, T.B. Neilsen, Near-field noise measurements of a high-performance military jet aircraft, *Noise Control Eng. J.* 60 (2012) 421–434.
[31] A.R. Bulsara, K. Lindenburg, K.E. Shuler, Spectral analysis of a nonlinear oscillator driven by random and periodic forces. i. linearized theory, *J. Stat. Phys.* 27 (1982) 787–808.
[32] R. Haiwu, X. Wei, M. Guang, F. Tong, Response of a duffing oscillator to combined deterministic harmonic and random excitation, *J. Sound Vib.* 242 (2001) 362–368.
[33] N.D. Anh, N.N. Hieu, The Duffing oscillator under combined periodic and random excitations, *Probab. Eng. Mech.* 30 (2012) 27–36.
[34] H.T. Zhu, S.S. Guo, Periodic response of a Duffing oscillator under combined harmonic and random excitations, *J. Vib. Acoust.* 137 (2015) 041015.
[35] A.H. Nayfeh, S.J. Serhan, Response statistics of non-linear systems to combined deterministic and random excitations, *Int. J. Non-Linear Mech.* 25 (1990) 493–509.
[36] B.F. Feeny, C.M. Yuan, Parametric identification of an experimental magneto-elastic oscillator, *J. Sound Vib.* 247 (2001) 785–806.
[37] T. Hikihara, T. Kawagoshi, An experimental study on stabilization of unstable periodic motion in magneto-elastic chaos, *Phys. Lett. A* 211 (1996) 29–36.
[38] A. Erturk, D.J. Inman, Broadband piezoelectric power generation on high-energy orbits of the bistable Duffing oscillator with electromechanical coupling, *J. Sound Vib.* 330 (2011) 2339–2353.
[39] N. Lajnef, R. Burgueño, W. Borchani, Y. Sun, A concept for energy harvesting from quasi-static structural deformations through axially loaded bilaterally constrained columns with multiple bifurcation points, *Smart Mater. Struct.* 23 (2014) 055005.
[40] J.B. Roberts, P.D. Spanos, *Random Vibration and Statistical Linearization*, Wiley, New York, 1990.
[41] R.A. Ibrahim, *Parametric Random Vibration*, Wiley, New York, 1985.
[42] N. Minorsky, *Nonlinear Oscillations*, ., D. Van Nordstrand Company, Inc., New York, 1962.
[43] C.W.S. To, *Nonlinear Random Vibration: Analytical Techniques and Applications*, CRC Press, London, 2012.
[44] R. Wiebe, S.M. Spottswood, Co-existing responses and stochastic resonance in post-buckled structures: a combined numerical and experimental study, *J. Sound Vib.* 333 (2014) 4682–4694.
[45] Q. He, M.F. Daqaq, New insights into utilizing bistability for energy harvesting under white noise, *J. Vib. Acoust.* 137 (2015) 021009.
[46] L. Gammaitoni, P. Hänggi, P. Jung, F. Marchesoni, Stochastic resonance, *Rev. Mod. Phys.* 70 (1) (1998) 223–287.
[47] T. Wellens, V. Shatokhin, A. Buchleitner, Stochastic resonance, *Rep. Progress. Phys.* 67 (2004) 45–105.
[48] F. Moss, Stochastic resonance: from the ice ages to the monkey's ear, in: Weiss Statistical Physics, G.H. (Ed.), *Contemporary Problems in Statistical Physics*, SIAM, Philadelphia, 1994. (ch. 5).
[49] M.I. Dykman, D.G. Luchinsky, R. Mannella, P.V.E. McClintock, N.D. Stein, N.G. Stocks, Stochastic resonance in perspective, *Il Nuovo Cimento* 17 (1995) 661–683.